

Geophysical Research Letters

RESEARCH LETTER

10.1002/2015GL065588

Key Points:

- We propose a tsunami forecasting method based on successive data assimilation
- Assimilation directly estimates tsunami height and velocity without using a source
- Simulation successfully estimates a tsunami using a planned tsunameter network

Supporting Information:

- Supporting Information S1
- Movie S1
- Movie S2

Correspondence to:

T. Maeda,
maeda@eri.u-tokyo.ac.jp

Citation:

Maeda, T., K. Obara, M. Shinohara, T. Kanazawa, and K. Uehira (2015), Successive estimation of a tsunami wavefield without earthquake source data: A data assimilation approach toward real-time tsunami forecasting, *Geophys. Res. Lett.*, 42, 7923–7932, doi:10.1002/2015GL065588.

Received 29 JUL 2015

Accepted 4 SEP 2015

Accepted article online 8 SEP 2015

Published online 3 OCT 2015

Successive estimation of a tsunami wavefield without earthquake source data: A data assimilation approach toward real-time tsunami forecasting

Takuto Maeda¹, Kazushige Obara¹, Masanao Shinohara¹, Toshihiko Kanazawa², and Kenji Uehira²

¹Earthquake Research Institute, University of Tokyo, Tokyo, Japan, ²National Research Institute for Earth Science and Disaster Prevention, Ibaraki, Japan

Abstract We propose a tsunami forecasting method based on a data assimilation technique designed for dense tsunameter networks. Rather than using seismic source parameters or initial sea surface height as the initial condition of for a tsunami forecasting, it estimates the current tsunami wavefield (tsunami height and tsunami velocity) in real time by repeatedly assimilating dense tsunami data into a numerical simulation. Numerical experiments were performed using a simple 1-D station array and the 2-D layout of the new S-net tsunameter network around the Japan Trench. Treating a synthetic tsunami calculated by the finite-difference method as observed data, the data assimilation reproduced the assumed tsunami wavefield before the tsunami struck the coastline. Because the method estimates the full tsunami wavefield, including velocity, these wavefields can be used as initial conditions for other tsunami simulations to calculate inundation or runup for real-time forecasting.

1. Introduction

Tsunami observations have advanced greatly in recent decades. The Deep-ocean Assessment and Reporting of Tsunami (DART) system [González *et al.*, 2005] measures tsunamis in the Pacific Ocean by using pressure gauges, and its data are transmitted by satellite for real-time tsunami forecasting [e.g., Titov *et al.*, 2005]. Around the Japanese islands, instruments linked to the shore by ocean bottom cables [e.g., Eguchi *et al.*, 1998; Hino *et al.*, 2001] have been used for tsunami observations for more than a decade. The recently developed Dense Ocean Floor Network System for Earthquake and Tsunamis [Baba *et al.*, 2013] in the Nankai trough provides tsunami measurements as well as broadband seismic data from the seafloor. Recently, Sheehan *et al.* [2015] succeeded in detecting the 2012 Haid Gwaii tsunami by dense ocean bottom tsunameter array in Cascadia. And the S-net, a new cabled network [Uehira *et al.*, 2012; Saito, 2013] (see Figure 1) currently being installed around the Japan Trench, covers a wide area of Japan's Pacific coast at a station spacing of 30–50 km, which is nearly as dense as land-based seismic networks such as Hi-net and K-NET [Okada *et al.*, 2004]. With its real-time data transmission, the S-net will be a powerful tool for forecasting tsunamis.

Because tsunamis propagate much more slowly (about 220 m/s at 5000 m depth) than seismic waves, early detection of tsunamis may enable timely evacuation of coastal areas if a tsunami is well characterized by offshore observations and if a tsunami forecast can be performed quickly enough. This idea underlies many approaches to real-time tsunami forecasting that utilize seismic tsunami and geodetic data sets. For example, Wang *et al.* [2012] used the W-phase solution from the Global Centroid-Moment-Tensor project to forecast tsunamis from the 11 April 2012 Sumatra earthquake. Titov *et al.* [2005] estimated source fault parameters from real-time offshore DART buoy data. Tsushima *et al.* [2009] proposed forecasting tsunamis by inverting the initial disturbance in sea height caused by earthquakes in pressure data from cabled ocean bottom instruments. Tsushima *et al.* [2012] incorporated real-time Global Navigation Satellite Systems data from the Japanese islands to speed up this process.

In very large earthquakes, the distribution of slip on the source faults has a significant effect on the resulting tsunamis [Goda *et al.*, 2014]. However, there is a large degree of uncertainty in estimating seismic source data [Mai *et al.*, 2007] that affects the accuracy of tsunami models. Using initial sea heights [Tsushima *et al.*, 2009, 2012; Saito *et al.*, 2011] rather than fault slip avoids the complexities of fault motions. In either case, however, the tsunami analysis is triggered by the detection of a seismic event. Therefore, these schemes may overlook

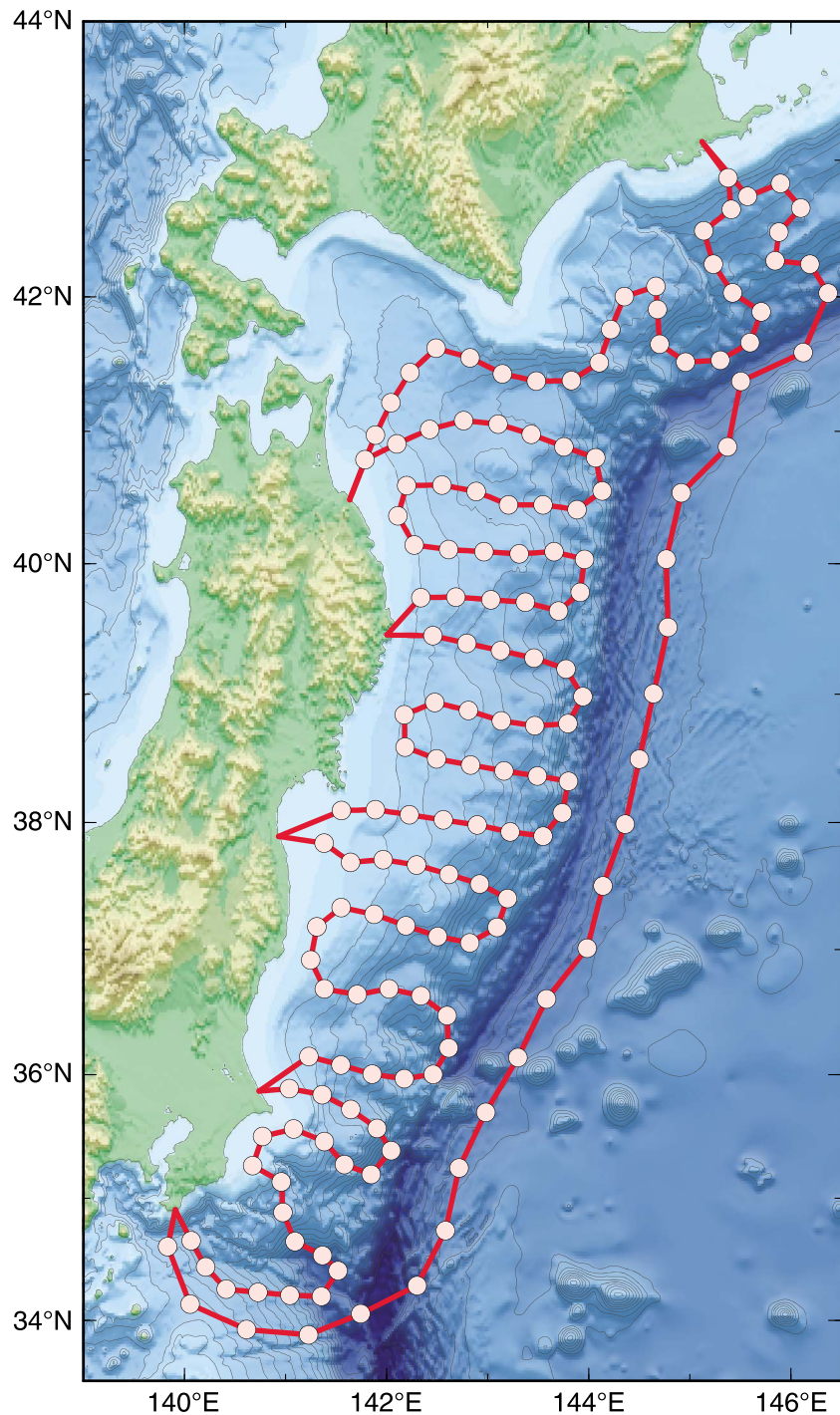


Figure 1. Planned configuration of the S-net showing sensor locations (circles) and cables (red lines). Bathymetric contour interval is 500 m.

unusual tsunamis, such as those caused by tsunami earthquakes or landslides, that are not accompanied by strong seismic records.

In this study, we tested an approach to tsunami forecasting that avoids the uncertainties of modeling a seismic source. Instead, we directly estimated the tsunami wavefield, including tsunami height and velocity, on the basis of real-time data from an ocean bottom network of tsunamieters by using data assimilation. This paper focuses on the procedure to extract a spatial tsunami wavefield from tsunamieter network data.

2. Data Assimilation of Tsunami Wavefields

The data assimilation procedure follows a method used in atmospheric science [Kalnay, 2003, section 5.4]. We adopted a simple 2-D linear long-wave (LLW) equation as the governing equation [e.g., Goto, 1984] for tsunamis observed in the deep ocean:

$$\begin{aligned}\frac{\partial \eta(x, y, t)}{\partial t} &= -\frac{\partial M(x, y, t)}{\partial x} - \frac{\partial N(x, y, t)}{\partial y} \\ \frac{\partial M(x, y, t)}{\partial t} &= -gD(x, y) \frac{\partial \eta(x, y, t)}{\partial x} \\ \frac{\partial N(x, y, t)}{\partial t} &= -gD(x, y) \frac{\partial \eta(x, y, t)}{\partial y},\end{aligned}\quad (1)$$

where η is the tsunami height, (M, N) are the vertically integrated horizontal velocity components of the tsunami in the x and y directions (hereafter referred to as the tsunami velocity), g is the gravitational acceleration constant (9.80665 m/s^2), and $D(x, y)$ is the sea depth. The model parameters to be estimated are tsunami height and tsunami velocity for the whole area of interest, represented as $\mathbf{x}_n = (\eta(n\Delta t, x, y), M(n\Delta t, x, y), N(n\Delta t, x, y))^T$ at discretized time steps $t = n\Delta t$. Given an estimated tsunami wavefield at the $(n-1)$ th time step, \mathbf{x}_{n-1}^a , the wavefield at the next time step can be forecast by integrating equation (1) with respect to time as $\mathbf{x}_n^f = \mathbf{F}\mathbf{x}_{n-1}^a$. The observed tsunami height at stations can be extracted from the true wavefield $\mathbf{x}_n^{\text{True}}$ by a sparse linear observation matrix \mathbf{H} with random noise field \mathbf{r} using the relation $\mathbf{y}_n = \mathbf{H}\mathbf{x}_n^{\text{True}} + \mathbf{r}$. In a numerical simulation, the tsunami height can be synthesized by applying the same observation matrix \mathbf{H} to the synthesized wavefield, which is expressed as $\mathbf{H}\mathbf{x}_n^f$. We assumed that matrix \mathbf{H} has a value of 1 at numerical grids of observation of tsunami height; all other components of \mathbf{H} are set to zero. Using these notations, we express the assimilation of the tsunami wavefield at time step n as

$$\mathbf{x}_n^a = \mathbf{x}_n^f + \mathbf{W}[\mathbf{y}_n - \mathbf{H}\mathbf{x}_n^f], \quad (2)$$

where \mathbf{W} is the weight matrix. This data assimilation expression can be interpreted as an estimation of the tsunami wavefield in two steps. In the first step, the tsunami wavefield is approximated by a forward numerical simulation, $\mathbf{x}_n^f = \mathbf{F}\mathbf{x}_{n-1}^a$. In the second step, the residual between the observed tsunami waveform and the simulation, $\mathbf{y}_n - \mathbf{H}\mathbf{x}_n^f$, is used as a correction that brings the assimilated wavefield closer to the true wavefield through an appropriate smoothing matrix \mathbf{W} . Once the tsunami wavefield is estimated through equation (2), the estimated wavefield can be used as the initial condition for forecasting the tsunami at the next time step, enabling data assimilation to be applied successively to a time series of continuous data.

In this scheme, the weight matrix \mathbf{W} is a key controlling factor for the quality of the assimilation. For evaluating \mathbf{W} , we relied on a simple optimal interpolation method [Kalnay, 2003, section 5.4]. Since we assumed that the observation matrix \mathbf{H} is linear and that the weight matrix \mathbf{W} does not depend on time, we can analytically estimate \mathbf{W} by minimizing the covariance matrix of $\langle \varepsilon^a \varepsilon^{aT} \rangle = \langle (\mathbf{x}_n^a - \mathbf{x}_n^{\text{True}})(\mathbf{x}_n^a - \mathbf{x}_n^{\text{True}})^T \rangle$ as a solution of the linear system

$$\mathbf{W}(\mathbf{R} + \mathbf{H}\mathbf{P}^f\mathbf{H}^T) = \mathbf{P}^f\mathbf{H}^T, \quad (3)$$

where $\mathbf{P}^f = \langle \varepsilon^f \varepsilon^{fT} \rangle$ and $\mathbf{R} = \langle \varepsilon^O \varepsilon^{OT} \rangle$ are the covariance matrices of the forward numerical simulation and the observations, respectively.

We assumed that observation error was uncorrelated among stations because observations are made independently, which simplified \mathbf{R} into a diagonal matrix whose diagonal component was the standard deviation of the observation error at each station. Assuming that the standard error between numerical grids is homogeneous in space, we obtain a simplified form of

$$\sum_{j=1}^m w_{gj} \left(\mu_{ij}^b + \delta_{ij} \rho_i \rho_j \right) = \mu_{gi}^b, \quad (4)$$

where w_{gj} is a components of the weight matrix \mathbf{W} , μ_{ij}^b is the correlation function of errors in numerical forecasts between two observational points (or computational grids), and ρ_i is the relative error of root-mean-square of observational error compared with the error in numerical forecasts. Readers are referred to the section 5.4.2 of Kalnay [2003] for the detail of the derivation of (4). We assumed Gaussian correlation

function as μ_{ij}^b with characteristic distance of 10 km. The choice of ρ_i controls the behavior of the data assimilation. In the following numerical test, we assumed $\rho_i=1$ as a result of trial and error. Equation (4) can be solved numerically in a standard way, such as by the Jacobi method [e.g., Press *et al.*, 1986], to obtain \mathbf{W} .

3. Numerical Experiment

3.1. Homogeneous 1-D Case

As the simplest case, we performed a numerical experiment incorporating data assimilation that used a 1-D homogeneous sea with a uniform depth. We assumed that the tsunami height was observed by 12 evenly spaced stations separated by 30 km, similar to the layout of the S-net cabled station network. First, a tsunami wave was simulated by solving the 1-D LLW tsunami wave equation by the finite-difference method with a Gaussian initial sea height at the elapsed time of 200 s and a characteristic source width of 30 km. Subsequently, the synthesized tsunami heights at 1 s intervals at the stations were treated as observational data. The wave height and velocity of the tsunami were then reconstructed at 1 s intervals by assimilation of these synthetic observations using equation (2).

Figure 2 shows the assumed and assimilated wavefields of tsunami height and tsunami velocity. The wavefields were reconstructed almost perfectly from the station data. Although sea heights at discrete stations were the only observed data used in this experiment, it successfully reconstructed both the wave height and the tsunami velocity, because the observed tsunami height was repeatedly fitted to the equation of motion through the assimilation equation (2).

The reproducibility of the tsunami wavefield decreased as wavelength decreased relative to the station separation. Figure 3 shows the tsunami height in 1-D tests with half-wavelength station spacing (Figure 3a) and with sparse observations (Figure 3b). The assimilation step introduced some artificial oscillation for a tsunami of shorter wavelength than the station separation. The simulation with sparse observations included no stations near the tsunami source. In that case, reverberations occurred in the tsunami source area but not in the area with observation stations. Assimilating tsunami data from just three stations, in the distance range 200–300 km, was sufficient to yield an accurate tsunami wavefield in the distance range 0–200 km even without additional observations.

We note that the numerical tests shown in Figures 2 and 3 are noise free. The effect of observation noise to the data assimilation is demonstrated in the Figure S1 in the supporting information. We added Gaussian random noise to the observations with different signal-to-noise ratio (Figures S1a–S1c). The signal-to-noise ratio is defined to as a ratio between average maximum amplitudes at distant stations and a standard deviation of Gaussian error. The quality of data assimilation became lower as increasing noise level as expected. However, even at high noise level of $S/N=50\%$, the main pulse of assumed tsunami is well assimilated. It is noteworthy that at high noise level case (Figure S1c), we can slightly reduce the effect of observation noise by increasing parameter ρ up to 2 (Figure S1d). It suggests that the fine choice of the parameter will be necessary in real-world applications.

3.2. Assimilating the 2011 Tohoku Earthquake Tsunami With a Dense Tsunameter Network

Next, we performed a more realistic test of the tsunami data assimilation scheme using the planned station layout of the S-net. All of the stations shown in Figure 1 were used as synthetic stations. We first simulated the tsunami at these stations caused by the 2011 Tohoku earthquake based on the initial source rupture model of Maeda *et al.* [2011], by using equation (1) and the finite-difference method. Then we reconstructed the tsunami wavefield by using the simulated tsunami traces at the S-net stations at 1 s intervals (Figure 4a).

Ocean bottom pressure gauges can only observe the distance between the sea surface and the seafloor. For great subduction zone events such as the Tohoku earthquake, coseismic deformation due to the fault motion affects these observations [e.g., Maeda *et al.*, 2013]. If we assume that the rupture process is negligibly short compared to the tsunami wave propagation and that the spatial dimension of the source fault sufficiently exceeds the sea height, then the initial sea height of the tsunami coincides with the coseismic deformation. Therefore, the pressure gauges will not record any immediate signal. For that reason, we subtracted the initial tsunami heights at the stations from the input tsunami data to make this simulation more realistic (Figure 4b).

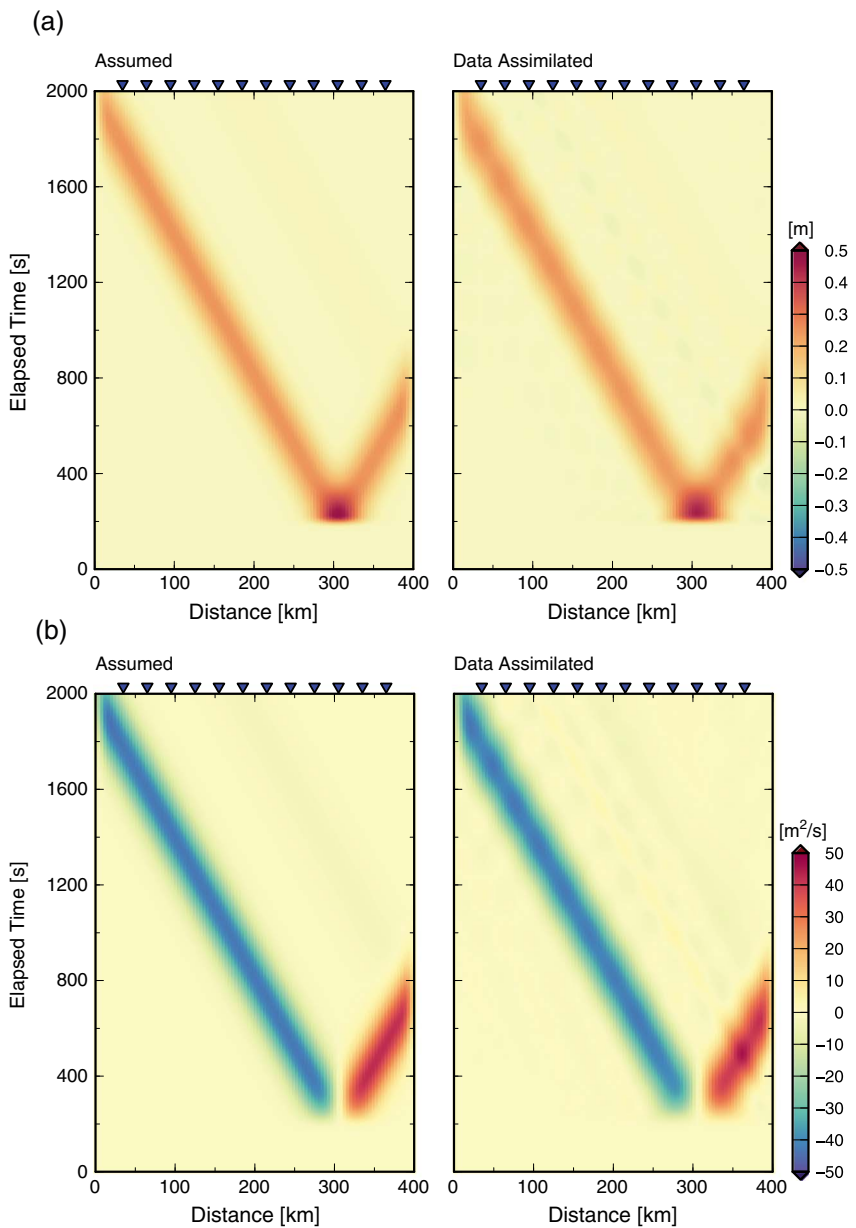


Figure 2. One-dimensional test of tsunami data assimilation showing assumed (left) and data-assimilated (right) tsunami wavefields for (a) tsunami height and (b) tsunami velocity. Station placement is indicated by inverted triangles at the top of the panels. Color scale for tsunami height and tsunami velocity is shown on right.

Results of the numerical experiment are shown in Figure 4c. As the tsunami initiated at $t = 0$ s, the assimilated field did not respond because the pressure gauge data could not detect the tsunami (Figure 4b). As the tsunami wave propagated outside of its source area, the data-assimilated tsunami wavefield started radiating tsunamis from each station. These quickly coalesced into a continuous wavefront that increasingly resembled the input data as time went on. As a result, the data-assimilated tsunami recovered the wavefront of the synthetic tsunami as it approached the coastline at $t = 1000$ s.

Our experiment produced an artificial negative offset due to coseismic deformation; however, it dissipated toward the Pacific Ocean as time elapsed. This occurred because the persistence of the offset does not obey equation (1), and there were relatively few constraining data from stations east of the Japan Trench. The tsunami wavefield was unaffected by this artifact on its western side along the coast.

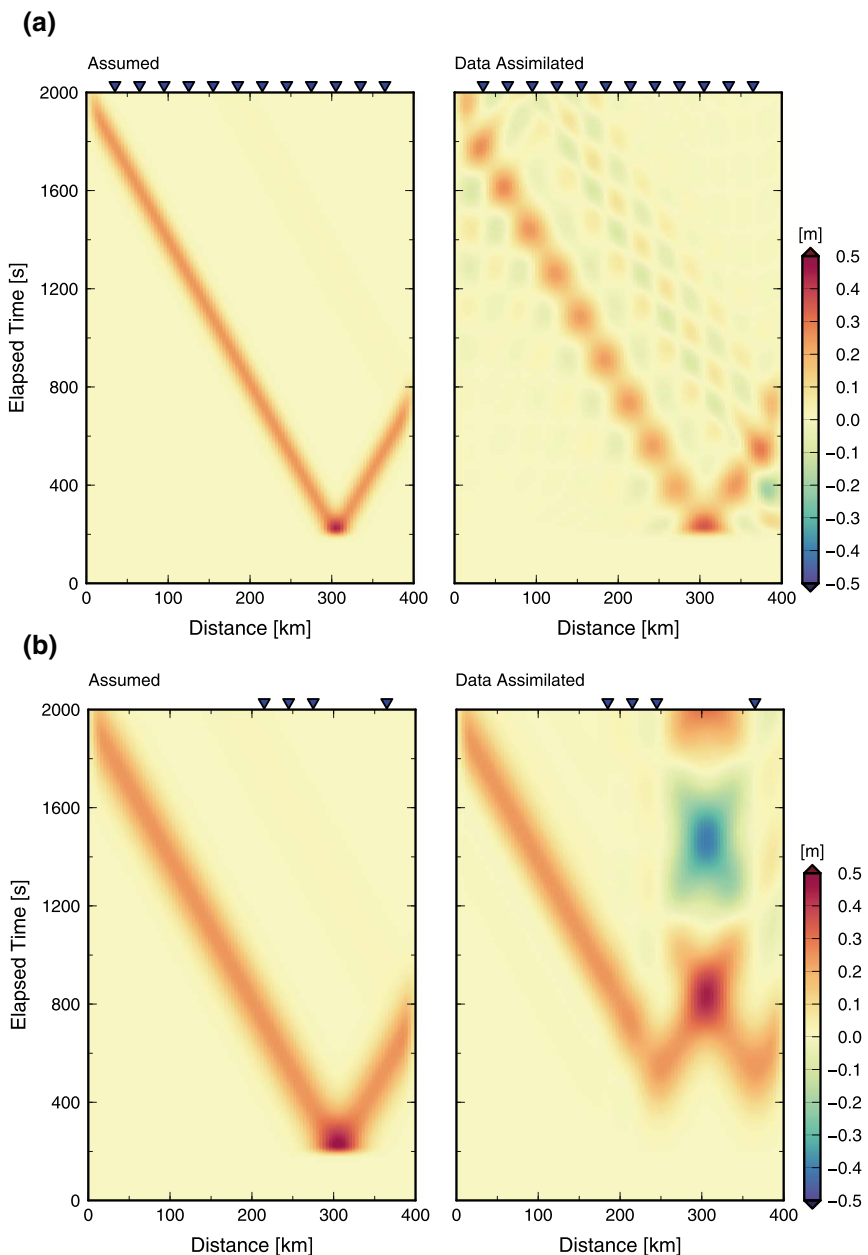


Figure 3. One-dimensional tests of tsunami data assimilation showing assumed (left) and data-assimilated (right) tsunami heights for relatively poor observations. (a) Relatively short wavelength compared to station separation. (b) Poor station coverage.

Computation speed is an important aspect of real-time tsunami estimation. The optimal interpolation method is so simple that this numerical test assimilated a tsunami wavefield for 1000 s of elapsed time in less than 200 s, faster than in real time, on a personal computer (equipped with an Intel Xeon E5620 2.93 GHz processor) without any parallelization. Therefore, this data assimilation method can be applied to current regional tsunami monitoring.

3.3. Possible Application to Far-Field Earthquakes

Recent observations with the DART ocean bottom tsunami network show that tsunamis from far-field earthquakes are systematically delayed with respect to numerical forecasts [Watada *et al.*, 2014]. The delay

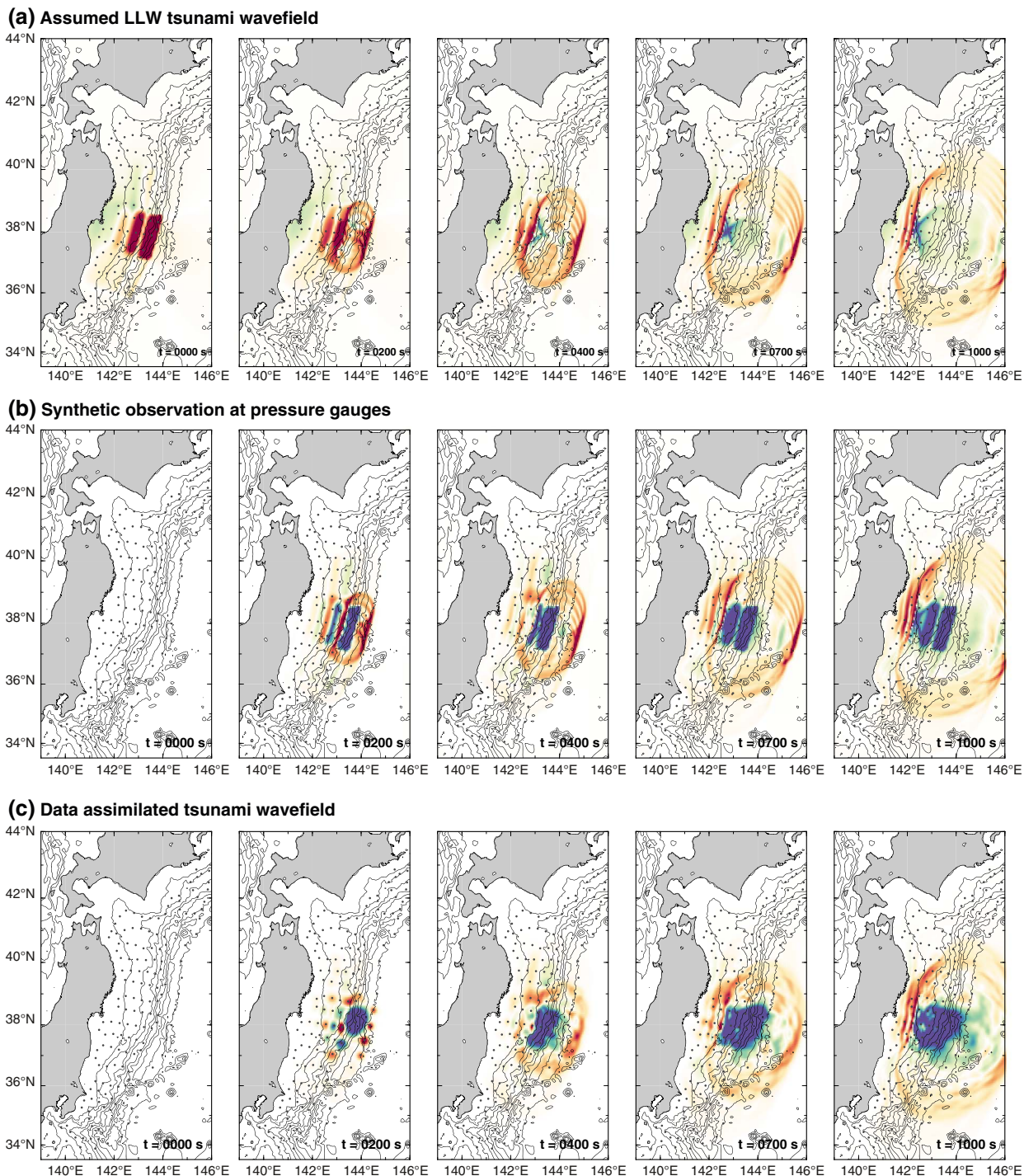


Figure 4. Experiment of tsunami data assimilation for the Tohoku earthquake at five time steps between $t = 0$ and $t = 1000$ s. (a) Assumed tsunami height calculated from the initial sea height model of Maeda *et al.* [2011]. (b) Synthetic tsunami data observed at pressure gauges (see text for explanation). (c) Data-assimilated tsunami wavefield based on input of Figure 4b at S-net stations. Bathymetric contour interval is 500 m. S-net stations used for the data assimilation are shown as black dots. Color scale of tsunami height is shown at right. A movie of this time sequence is provided in the supporting information (Movie S1).

is thought to be caused by interaction between the seawater column and the seafloor [Watada, 2013] and by density variations in seawater [Tsai *et al.*, 2013]. To take this delay into account, Inazu and Saito [2013] introduced a small empirical correction to the tsunami velocity to improve forecasts of tsunami arrivals from data at distant stations.

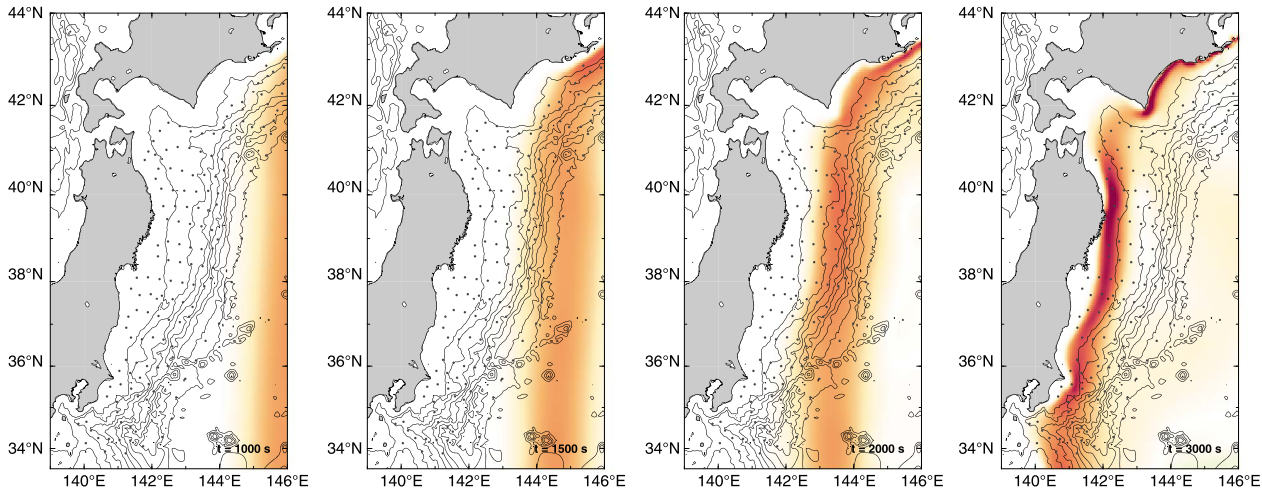
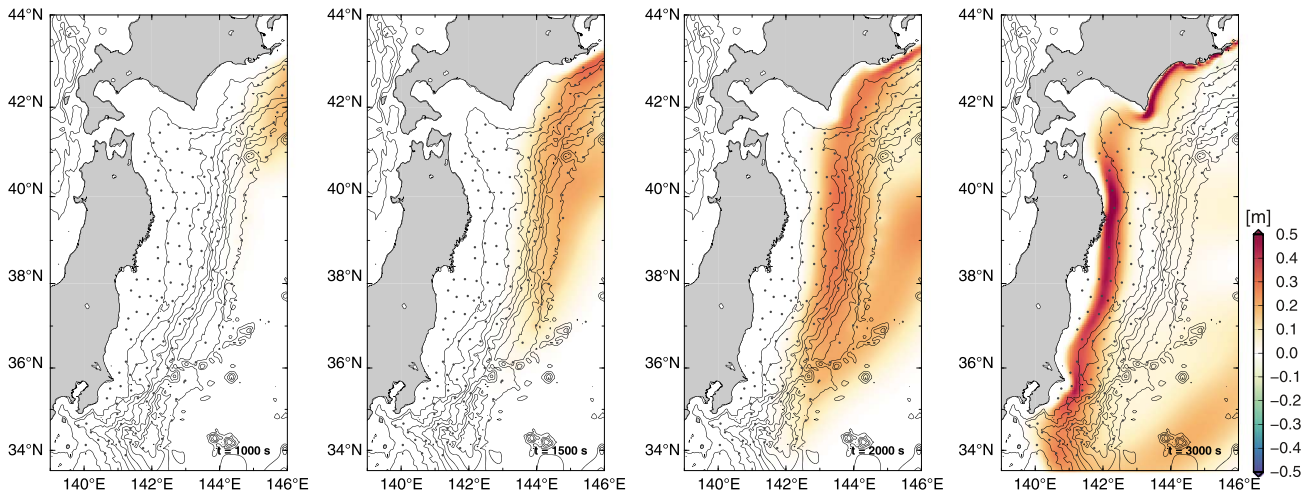
(a) Assumed tsunami wavefield**(b) Data assimilated tsunami wavefield**

Figure 5. Simulation of data assimilation for a tsunami from a far-field source, modeled as a long-wavelength plane wave. (a) Assumed wavefield at $t = 1000, 1500, 2000$, and 3000 s. (b) Data-assimilated wavefield. Bathymetry contour interval is 500 m. S-net stations used for the data assimilation are shown as black dots. Color scale of tsunami height is shown at right. A movie of this time sequence is provided in the supporting information (Movie S2).

The data assimilation method may provide an alternative approach to accurately forecast the arrival of far-field tsunamis from near-field dense observations. In our test of this possibility (Figure 5), we assumed a plane wave to represent the arrival of a tsunami from a far-field earthquake to the S-net. The assumption of a far-field source meant that we did not need to consider seafloor offsets due to coseismic deformation. As the tsunami propagated toward Japan, the data-assimilated wavefield gradually reproduced the tsunami before it reached the coast. Although there was a spurious reflection eastward due to the lack of tsunamieters on the seaward side of the model, it did not affect the westward propagation of the tsunami. Because the data assimilation approach does not rely on source information, and because it captures far-field tsunamis in a near-field dense network, it should avoid the problem of delay in long-range tsunami propagation that degrades forecasts.

4. Discussion

Because the data assimilation method does not need to estimate an initial condition at the tsunami source, even a partial network of suitable density can be used for an in situ tsunami estimation. For example, our test

showed that even if the regional tsunameter network is distant from the source region and if its size is too small to cover the entire earthquake source area, data assimilation can succeed in estimating the portion of the tsunami wave passing through the array (Figure 3). Tsunami estimation that does not rely on a source may have a great advantage in monitoring tsunamis from tsunami earthquakes, landslides, or other unconventional origins. For such purpose, it should be preferable to operate tsunami data assimilation continuously irrespective to the occurrence of large earthquake.

This paper focused on estimating the tsunami wavefield in real time by using data assimilation. Because the product is the full wavefield, including the wave height and velocity, these will be available as initial conditions for other tsunami forecasting methods, such as tFISH [*Tsushima et al.*, 2009]. Because the forecasting stage is independent from the data assimilation stage, nonlinear tsunami equations can be combined with data assimilation to estimate tsunami inundation or runup [*Gusman et al.*, 2014].

In the numerical experiment of the 2011 Tohoku earthquake, there was a systematic discrepancy between assumed sea height and data assimilation coming from the nature of observation by pressure gauges at the ocean floor, although the effect was relatively small. We assumed sea height was observed through the definition of observation matrix \mathbf{H} ; however, there are systematic offset due to the coseismic deformation. In addition, the pressure gauge record may be affected by seismic waves or ocean acoustic waves accompanied with large near-field earthquake. These effects should be clarified in more detail through real data application and numerical tests with realistic tsunami simulation including seismic waves and coseismic deformations [e.g., *Maeda and Furumura*, 2013; *Maeda et al.*, 2013] in future studies.

Although we assumed the weight matrix to be static in time in the optimal interpolation method, the Kalman filter approach [e.g., *Kalnay*, 2003, section 5] can handle the time-dependent error covariance. The Kalman filtering may be more appropriate on tracking uncertainties of tsunami forecast through better error estimation; however, the computational cost on updating weight matrix will become extraordinary large to use the Kalman filter for tsunami data assimilation in real time. Adopting techniques to reduce computational cost, such as a partitioned Kalman filter [*Fukumori*, 2001], may be useful for more precise error handling of the real-time data assimilation of tsunami.

Our numerical tests showed that the quality of the data assimilation strongly depends on the relation between station separation and tsunami wavelength. Tsunamis generally have longer wavelengths in the deep ocean. This result implies that if we can successfully assimilate tsunami wavefields with a dense tsunameter network in offshore areas where tsunamis have long wavelengths, short-wavelength tsunamis in coastal areas can be well reproduced or forecast through the data assimilation technique.

Estimating the tsunami wavefield in the deep ocean has another advantage. Tsunami amplitudes are generally very small in the deep ocean, which allows us to use a simple tsunami equation without nonlinear terms. This linearity of the time-marching equation is necessary for using the optimal interpolation method for data assimilation. This simplification greatly reduces the computation cost of tsunami wavefield estimation, favoring its use for real-time forecasting. However, frequency dispersion may have important effects on tsunamis in the deep ocean. Incorporation of linear dispersive tsunami models [e.g., *Saito et al.*, 2010] may further improve the quality of data assimilation. If such dispersive tsunami are dominated, the data assimilation based on LLW equation may mistreat it as random error that does not obey the assumed equation, which may lead systematic bias on tsunami forecasting. Because of a significant cost in computational loads for dispersive tsunami, large-scale massively parallel computation [e.g., *Oishi et al.*, 2015] will be necessary in future studies of more accurate real-time tsunami estimation.

Acknowledgments

We used the gridded bathymetry data set JTOPO30v2 provided by the Marine Information Research Center, Japan Hydrographic Association. T.M. is supported by Japan Society for the Promotion of Science (JSPS) KAKENHI grant 15K16306. We thank reviewers for careful reading and fruitful suggestions that improved the manuscript.

The Editor thanks three anonymous reviewers for their assistance in evaluating this paper.

References

- Baba, T., N. Takahashi, and Y. Kaneda (2013), Near-field tsunami amplification factors in the Kii Peninsula, Japan for Dense Oceanfloor Network for Earthquakes and Tsunamis (DONET), *Mar. Geophys. Res.*, 35(3), 319–325, doi:10.1007/s11001-013-9189-1.
- Eguchi, T., Y. Fujinawa, E. Fujita, S. Iwasaki, I. Watabe, and H. Fujiwara (1998), A real-time observation network of ocean-bottom-seismometers deployed at the Sagami trough subduction zone, central Japan, *Mar. Geophys. Res.*, 20(2), 73–94, doi:10.1023/A:1004334021329.
- Fukumori, I. (2001), A partitioned Kalman filter and smoother, *Mon. Weather Rev.*, 130, 1370–1383, doi:10.1175/1520-0493(2002)130<1370:APKFAS>2.0.CO;2.
- Goda, K., P. Mai, T. Yasuda, and N. Mori (2014), Sensitivity of tsunami wave profiles and inundation simulations to earthquake slip and fault geometry for the 2011 Tohoku earthquake, *Earth Planets Space*, 66(1), 105, doi:10.1186/1880-5981-66-105.
- González, F. I., E. N. Bernard, C. Meinig, M. C. Eble, H. O. Mofjeld, and S. Stalin (2005), The NTHMP tsunameter network, *Nat. Hazards*, 35, 25–39, doi:10.1007/s11040-3607-8_2.

- Goto, C. (1984), Equations of nonlinear dispersive long waves for a large Ursell number (in Japanese with English abstract), *J. Hydraul. Coastal Environ. Eng.*, 351, 193–201.
- Gusman, A. R., Y. Tanioka, B. T. Maclnnes, and H. Tsushima (2014), A methodology for near-field tsunami inundation forecasting: Application to the 2011 Tohoku tsunami, *J. Geophys. Res. Solid Earth*, 119, 8186–8206, doi:10.1002/2014JB010958.
- Hino, R., Y. Tanioka, T. Kanazawa, S. Sakai, M. Nishino, and K. Suyehiro (2001), Micro-tsunami from a local interplate earthquake detected by cabled offshore tsunami observation in northeastern Japan, *Geophys. Res. Lett.*, 28(18), 3533–3536, doi:10.1029/2001GL013297.
- Inazu, D., and T. Saito (2013), Simulation of distant tsunami propagation with a radial loading deformation effect, *Earth Planets Space*, 65(8), 835–842, doi:10.5047/eps.2013.03.010.
- Kalnay, E. (2003), *Atmospheric Modeling, Data Assimilation, and Predictability*, Cambridge Univ. Press, Cambridge.
- Maeda, T., and T. Furumura (2013), FDM simulation of seismic waves, ocean acoustic waves, and tsunamis based on tsunami-coupled equations of motion, *Pure Appl. Geophys.*, 170(1–2), 109–127, doi:10.1007/s00024-011-0430-z.
- Maeda, T., T. Furumura, S. Sakai, and M. Shinohara (2011), Significant tsunami observed at ocean-bottom pressure gauges during the 2011 off the Pacific coast of Tohoku earthquake, *Earth Planets Space*, 63(7), 803–808, doi:10.5047/eps.2011.06.005.
- Maeda, T., T. Furumura, S. Noguchi, S. Takemura, S. Sakai, M. Shinohara, K. Iwai, and S. J. Lee (2013), Seismic- and tsunami-wave propagation of the 2011 Off the Pacific Coast of Tohoku earthquake as inferred from the tsunami-coupled finite-difference simulation, *Bull. Seismol. Soc. Am.*, 103(2B), 1456–1472, doi:10.1785/0120120118.
- Mai, P. M., J. Burjanek, B. Delouis, G. Festa, C. Francois-Holden, D. Monelli, T. Uchide, and J. Zahradnk (2007), Earthquake source inversion blindtest: Initial results and further developments, *EOS Trans. AGU*, 88(52), Fall Meet. Suppl., Abstract SS3C-08.
- Oishi, Y., F. Imamura, and D. Sugawara (2015), Near-field tsunami inundation forecast using the parallel TSUNAMI-N2 model: Application to the 2011 Tohoku-Oki earthquake combined with source inversions, *Geophys. Res. Lett.*, 42, 1083–1091, doi:10.1002/2014GL062577.
- Okada, Y., K. Kasahara, S. Hori, K. Obara, S. Sekiguchi, H. Fujiwara, and A. Yamamoto (2004), Recent progress of seismic observation networks in Japan, *Earth Planets Space*, 56, xv–xxviii, doi:10.1186/BF03353076.
- Press, W. H., B. P. Flannery, S. A. Teukolsky, and W. T. Vetterling (1986), *Numerical Recipes: The Art of Scientific Computing*, Cambridge Univ. Press, New York.
- Saito, T. (2013), Dynamic tsunami generation due to sea-bottom deformation: Analytical representation based on linear potential theory, *Earth Planets Space*, 65(12), 1411–1423, doi:10.5047/eps.2013.07.004.
- Saito, T., K. Satake, and T. Furumura (2010), Tsunami waveform inversion including dispersive waves: The 2004 earthquake off Kii Peninsula, Japan, *J. Geophys. Res.*, 115(6), 1–12, doi:10.1029/2009JB006884.
- Saito, T., Y. Ito, D. Inazu, and R. Hino (2011), Tsunami source of the 2011 Tohoku-Oki earthquake, Japan: Inversion analysis based on dispersive tsunami simulations, *Geophys. Res. Lett.*, 38, L00G19, doi:10.1029/2011GL049089.
- Sheehan, A. F., A. R. Gusman, M. Heidarzadeh, and K. Satake (2015), Array observations of the 2012 Haida Gwaii tsunami using Cascadia initiative absolute and differential seafloor pressure gauges, *Seismol. Res. Lett.*, 86(5), doi:10.1785/0220150108.
- Titov, V. V., F. I. González, E. N. Bernard, M. C. Eble, H. O. Mofield, J. C. Newman, and A. J. Venturato (2005), Real-time tsunami forecasting: Challenges and solutions, *Nat. Hazards*, 35, 41–58, doi:10.1007/s10642-005-0367-8_3.
- Tsai, V. C., J. P. Ampuero, H. Kanamori, and D. J. Stevenson (2013), Estimating the effect of Earth elasticity and variable water density on tsunami speeds, *Geophys. Res. Lett.*, 40, 492–496, doi:10.1002/grl.50147.
- Tsushima, H., R. Hino, H. Fujimoto, Y. Tanioka, and F. Imamura (2009), Near-field tsunami forecasting from cabled ocean bottom pressure data, *J. Geophys. Res.*, 114, B06309, doi:10.1029/2008JB005988.
- Tsushima, H., R. Hino, Y. Tanioka, F. Imamura, and H. Fujimoto (2012), Tsunami waveform inversion incorporating permanent seafloor deformation and its application to tsunami forecasting, *J. Geophys. Res.*, 117, B03311, doi:10.1029/2011JB008877.
- Uehira, K., et al. (2012), Ocean bottom seismic and tsunami network along the Japan Trench, AGU Fall Meeting, Abstract OS41C-1736.
- Wang, D., et al. (2012), Real-time forecasting of the April 11, 2012 Sumatra tsunami, *Geophys. Res. Lett.*, 39, L1960, doi:10.1029/2012GL053081.
- Watada, S. (2013), Tsunami speed variations in density-stratified compressible global oceans, *Geophys. Res. Lett.*, 40, 4001–4006, doi:10.1029/2012GL053081.
- Watada, S., S. Kusumoto, and K. Satake (2014), Traveltime delay and initial phase reversal of distant tsunamis coupled with the self-gravitating elastic Earth, *J. Geophys. Res. Solid Earth*, 119, 4287–4310, doi:10.1002/2013JB010841.